Electrochimica Acta 469 (2023) 143117

Contents lists available at ScienceDirect

Electrochimica Acta

journal homepage: www.journals.elsevier.com/electrochimica-acta

# Electrochemical insight on the nitrogen-rich, weakly aromatic cyclic triimidazole multifunctional system expanded with pyridine or thiophene terminals

Daniele Malpicci [a,b], Silvia Rosa Araneo [a], Serena Arnaboldi [a], Elena Cariati [a,b], Alessandra Forni [b], Sara Grecchi [a], Elena Lucenti [b], Daniele Marinotto [b], Daniele Maver [a,b], Patrizia Romana Mussini [a,*]

[a] Dipartimento di Chimica, Università degli Studi di Milano, Via Golgi 19, Milano 20133, Italy
[b] Istituto di Scienze e Tecnologie Chimiche "Giulio Natta" (SCITEC), CNR, Via Golgi 19, Milano 20133, Italy

ARTICLE INFO

*Keywords:*
Electrochemistry of cyclic triimidazole **TT** derivatives
**TT** functionalization with pyridine, thiophene or bithiophene terminals
Effects of terminal nature and number
Electrodeposition of **TT**-tetrathiophene films
Electrochemistry and spectroelectrochemistry of **TT**-tetrathiophene films

ABSTRACT

Cyclic triimidazole **TT** and its derivatives are gaining increasing attention for their multifaceted properties spanning from photoluminescence to supramolecular chemistry and biological activity. **TTs** structure-property relationships can be rationalized with the aid of electrochemical techniques that can also afford a precious tool to transfer molecular properties to molecular materials. An attracting study case is provided by **TT** derivatives with an increasing number of heteroaromatic terminals, either pyridine (popular protonation-sensitive capping agent) or thiophene/bithiophene ones (promoting coupling processes). An exhaustive voltammetry investigation, integrated by (and in some cases combined with) absorption and emission spectroscopy and supported by theoretical calculations, highlights the modulation of the electronic/redox properties as a function of the terminal nature and multiplicity. Moreover, a couple of first examples of **TT** derivatives successfully electrooligomerizable into electrochemically and spectroscopically highly active films, is reported. This can be regarded as an attractive first step in the perspective of electrochemically developing molecular materials endowed with **TT** functional properties combined with high electroactivity.

## 1. Introduction

Organic chromophores with long-lived emissive properties in the solid state like Room Temperature Phosphorescence (RTP) are highly pursued by the scientific community due to their potential applications in several fields such as bioimaging [1–4], anti-counterfeiting [5–7], and sensing [8]. In this context, triazine-based derivatives with the heteroaromatic central core acting as an acceptor have produced multifunctional emitters with interesting performances and persistent RTP under ambient conditions [9–13].

A fascinating member of the triazine family is represented by triimidazo[1,2-*a*:1′,2′-*c*:1″,2″-*e*][1,3,5]triazine or cyclic triimidazole (hereafter **TT**, Scheme 1) and its derivatives, which have recently gained increasing attention for their multifaceted properties spanning from photoluminescence to supramolecular chemistry and biological activity [14–21]. **TT** has been known since 1973 [22]; however, the tedious synthetic protocols for its isolation constituted a major impediment until a simple procedure for its preparation in good yields has been reported [23], allowing further investigations on its properties and reactivity.

As for its luminescence features, the family of triimidazotriazines (**TTs**) exhibits a complex excitation dependent photoluminescence comprising dual fluorescence, molecular phosphorescence and supramolecular room temperature phosphorescence (RTP) [15,19,21,24–29].

Concerning **TT** coordination abilities, the presence of three nitrogen atoms available for coordination has paved the way in the use of **TT** for the preparation of Cu(I) and Ag(I) coordination networks where it behaves as a mono-, bi-, and tridentate ligand, giving rise to one-, two-, and three-dimensional (1D, 2D, 3D) coordination polymeric networks of different topologies [16,18]. Furthermore, **TT**, its positional isomer (**iso-TT**, having one imidazole ring with 1,5- instead of 1,2-annelation, Scheme 1) and some pyridine-**TT** derivatives have been successfully employed for the synthesis of Cu(I), Cu(II), Zn(II) and Cd(II) complexes

* Corresponding author.
*E-mail address:* patrizia.mussini@unimi.it (P.R. Mussini).

https://doi.org/10.1016/j.electacta.2023.143117
Received 27 April 2023; Received in revised form 25 August 2023; Accepted 29 August 2023
Available online 30 August 2023

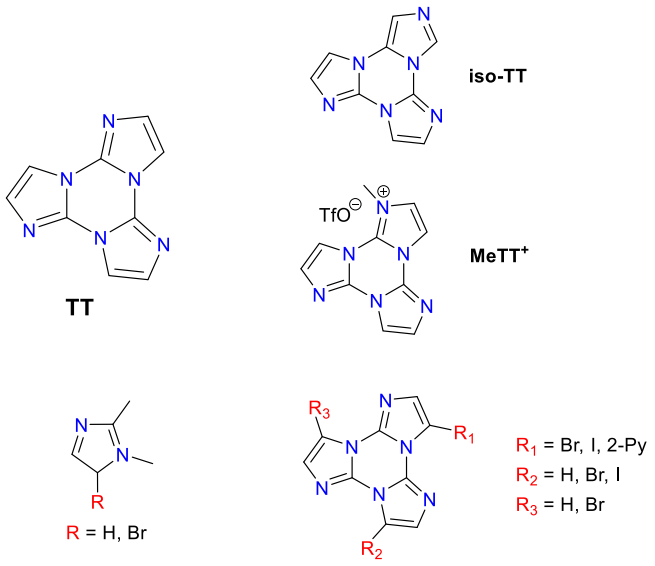


**Scheme 1.** The first electrochemically investigated set of **TT** derivatives and related model compounds [33].

and/or coordination polymers [17,30–32].

Finally, very recently, based on the observation that triazinic functionalities are frequently used in the biological field, pyrene-substituted **TT** has been successfully tested for cellular and bacterial bioimaging [19] while cyclic triimidazole derivatives functionalized with methylated pyridines or guanidines moieties have shown high affinity to bind to G-quadruplexes from both telomeric and oncogene promoter sequences [20].

In this frame, to enable rational design and optimized application of triimidazotriazine derivatives for specific applications, a deeper insight on their structure-property relationships is needed, for which aim electrochemistry represents a fundamental tool. However, to our knowledge only a single study discussing the electrochemistry of a systematic set of **TT** derivatives (Scheme 1) has so far appeared, on this Journal, coauthored by some of us [33].

In such investigation, mainly performed in dimethylformamide, DMF, polar solvent, the parent cyclic **TT** system was found to undergo oxidative as well as reductive electron transfer only at extreme potentials in the wide operating window, with the three imidazole units behaving as three nearly independent redox sites (of long known little electrochemical activity [34], although electrochemical oxidation of unsubstituted imidazole can result in N,N'-oligomerization [35]). Both observations supported the assumption of a vanishing heteroannular aromaticity along this nitrogen-rich 18 π-electron system [33,36]. Interestingly, asymmetric isomer **iso-TT** appeared more reactive,

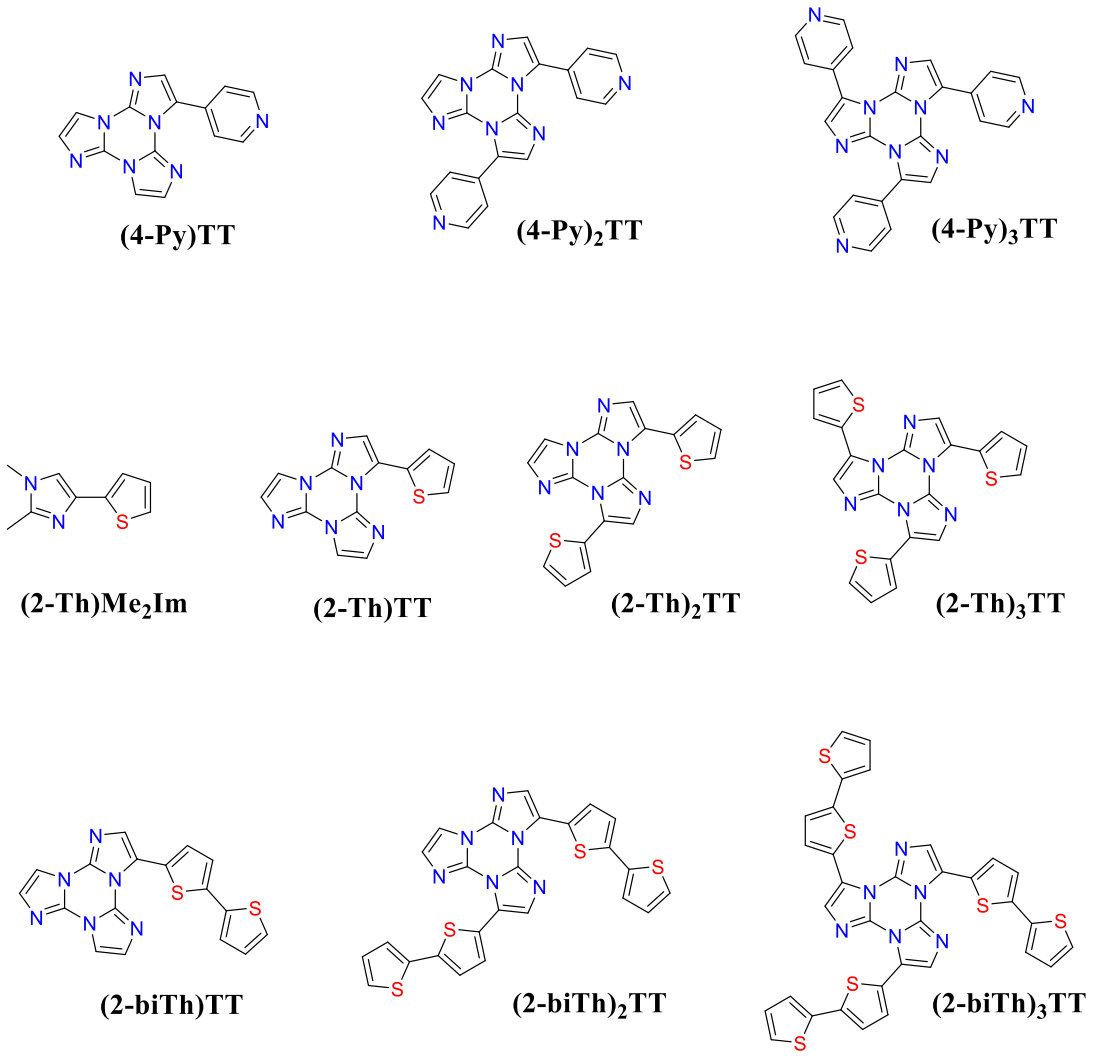


**Scheme 2.** The pyridine-, thiophene- or (bi)thiophene-terminated **TT** derivative set, also including a related model molecule, investigated in the present work.

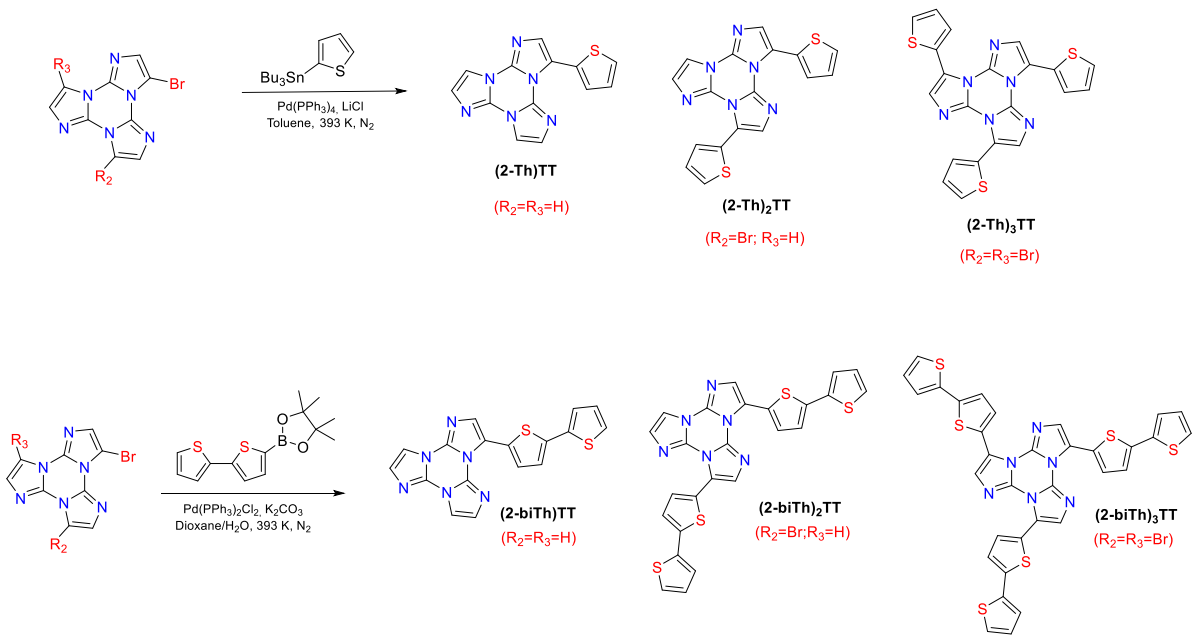


**Scheme 3.** Synthetic paths for the preparation of thienyl- and bithienyl-terminated derivatives.

undergoing at a milder potential its first oxidation, localized on the differently 1,5-annelated imidazole ring, while reduction, centered on the remaining two almost equivalent 1,2-annelated moieties, remained located at a potential similar to the major isomer one [33]. In the brominated derivative series, the electrochemical cleavage of the C–X bond is only slightly influenced by increasing the number of halogens from one to three. These findings further strengthened the hypothesis that each imidazole unit in the cyclic trimer acts as an almost independent redox site, with very poor heteroannular aromaticity [33]. **TT** conversion into an alkylated salt, making a N site electron poorer, resulted of course in a huge positive shift of the first reduction potential, as in similar cases (*e.g.* [37]).

Considering the above outlined multipurpose abilities and applicative perspectives of the **TT** building block, an attractive development

**Table 1**
A synopsis of CV results for pyridine-, thiophene- and bithiophene-functionalized **TT** systems as well as for some related benchmark molecules, compared with key parameters obtained from UV-Vis absorption spectroscopy as well as DFT calculations. Electrochemical and UV-Vis data are in DMF solvent unless otherwise specified.[#] In different media [40], normalized *vs* the $Fc^+|Fc$ intersolvental reference couple.[a] In $CH_3CN$ solvent.[b] In $CH_2Cl_2$ solvent.[c] First relative maximum.

| | $E_{p,c}$ *vs* $Fc^+\|Fc$ /V | $E_{p,a}$ *vs* $Fc^+\|Fc$ /V | $E_{LUMO}$ /eV | $E_{HOMO}$ /eV | $E_{g,\ EC}$ /V | $\lambda_{max}$ ($\lambda_{onset}$) / nm | $E_{g\ UV\text{-}vis}$ /eV | $E_{LUMO,\ DFT}$ /eV | $E_{HOMO,\ DFT}$ /eV | $E_{g,\ DFT}$ /eV |
|---|---|---|---|---|---|---|---|---|---|---|
| **$Me_2Im$** | *n.d.* | +1.00 [33] | | | | | | | | |
| **TT** | *-3.25*[33] | *+1.15* [33] | | | *4.4* | 260[c] (294) | 4.8 (4.2) | -0.80 | -6.83 | 6.03 |
| | | +1.38[a] [33] | | | | | | | | |
| **Py** | *-3.10* [38] | | | | | | | | | |
| **(2-Py)TT** | -2.8 [33] | +1.07 [33] | -2.00 | -5.87 | 3.87 | | | -1.47 | -6.41 | 4.94 |
| **(4-Py)TT** | -2.64 | *[1.7]* | -2.16 | *n.d.* | *n.d.* | 289 (331) | 4.30 (3.75) | -1.58 | -6.76 | 5.18 |
| | -2.92 | | | | | | | | | |
| **$(4\text{-Py})_2$TT** | -2.60 | *[1.7]* | -2.20 | *n.d.* | *n.d.* | 286 (333) | 4.34 (3.73) | -1.76 | -6.84 | 5.08 |
| | -2.85 | | | | | | | | | |
| | -2.95 | | | | | | | | | |
| **$(4\text{-Py})_3$TT** | -2.54 | *[1.8]* | -2.26 | *n.d.* | *n.d.* | 284 (333) | 4.39 (3.73) | -1.85 | -6.95 | 5.10 |
| | -2.81 | | | | | | | | | |
| | -2.91 | | | | | | | | | |
| **Th[#]** | -3.73 | +1.33 | -1.07 | -6.13 | 5.06 | | | | | |
| **α-$Th_2$[#]** | -2.84 | +0.88 | -1.96 | -5.68 | 3.72 | | | | | |
| **α-$Th_4$[#]** | -2.34, -2.64 | +0.37 | -2.46 | -5.17 | 2.71 | | | | | |
| **(2-Th)$Me_2$Im** | -3.21 | +0.64 | -1.59 | -5.44 | 3.85 | | | -0.87 | -5.9 | 5.03 |
| **(2-Th)TT** | -2.92 | +0.84 | -1.88 | -5.64 | 3.76 | 291 *(380)* | 4.27 *(3.27)* | -1.31 | -6.17 | 4.86 |
| **$(2\text{-Th})_2$TT** | -2.88 | +0.82 | -1.92 | -5.62 | 3.70 | 293 (351) | 4.22 (3.54) | -1.39 | -6.14 | 4.75 |
| **$(2\text{-Th})_3$TT** | -2.82 | +0.88 | -1.98 | -5.68 | 3.70 | 293 (351) | 4.24 (3.54) | -1.38 | -6.16 | 4.78 |
| **(2-biTh)TT** | -2.60 | 0.65 | -2.2 | -5.45 | 3.25 | 346 | 3.59 | -1.75 | -5.78 | 4.03 |
| | -2.88 | *0.69* | | | | | | | | |
| | -2.63[a] | 0.63 [a] | -2.17[a] | -5.43[a] | 3.26[a] | | | | | |
| | -2.87[a] | 0.78 [a] | | | | | | | | |
| | *-2.7*[b] | 0.67 [b] | -2.1 [b] | -5.47[b] | 3.37[b] | 339[b] | 3.66[b] | | | |
| **$(2\text{-biTh})_2$TT** | ~-2.65[b] | 0.65[b] | -2.15 [b] | -5.45[b] | 3.30[b] | 341[b] | 3.64[b] | -1.81 | -5.79 | 3.98 |
| **$(2\text{-biTh})_3$TT** | ~-2.62 [b] | 0.65[b] | -2.18 | -5.45[b] | 3.27[b] | 342[b] | 3.63[b] | -1.80 | -5.80 | 4.00 |

**Table 2**
A synopsis of absorption and emission data at 298 K for pyridine-, thiophene- and bithiophene-functionalized **TT** systems.

| | $\lambda_{abs}$ / nm | | $\varepsilon$[a] / ($dm^3$ $mol^{-1}$ $cm^{-1}$) | $\lambda_{em}$ / nm | | Stokes shifts / nm | | Average lifetime[b] $\tau_{av}$ / ns | Quantum yield Φ |
|---|---|---|---|---|---|---|---|---|---|
| | $CH_2Cl_2$ | DMF | | $CH_2Cl_2$ | DMF | $CH_2Cl_2$ | DMF | | |
| **TT** | 260[c] | 265 | | [d] | 329, 425 | | | | |
| **(4-Py)TT** | 284 | 289 | $8.9 \times 10^3$ | 345 | 356 | 61 | 67 | 0.73 | 23 |
| **$(4\text{-Py})_2$TT** | 280 | 286 | $29 \times 10^3$ | 359 | 393 | 79 | 107 | 2.36 | 26 |
| **$(4\text{-Py})_3$TT** | 271 | 284 | $41 \times 10^3$ | 371 | 401 | 100 | 117 | 2.27 | 25 |
| **(2-Th)$Me_2$Im** | | | $8.2 \times 10^3$ | | | | | | |
| **(2-Th)TT** | 286 | 291 | $8.4 \times 10^3$ | 364[e] | 366 | 78 | 75 | n.d. | 11 |
| **$(2\text{-Th})_2$TT** | 287 | 293 | $16 \times 10^3$ | 367[e] | 392 | 80 | 99 | 1.05 | 9 |
| **$(2\text{-Th})_3$TT** | 288 | 293 | $28 \times 10^3$ | 379[e] | 431[d] | 91 | 138 | 1.28 | 6 |
| **(2-biTh)TT** | 339 | 346 | $16 \times 10^3$ | 433[e] | 436[e] | 94 | 90 | 0.22 | 9 |
| **$(2\text{-biTh})_2$TT** | 341 | 346 | $23 \times 10^3$ | 434[c] | 438[c] | 93 | 92 | 0.22 | 11 |
| **$(2\text{-biTh})_3$TT** | 342 | 347 | $63 \times 10^3$ | 440[e] | 439[e] | 98 | 92 | n.d. | 12 |
| **Poly$(biTh)_2$TT** | ~370–420[g] | | | | | | | | |
| | ~740–820[h] | | | | | | | | |
| | ~1120-1180[i] | | | | | | | | |
| **Poly$(byTh)_3$TT** | ~380–420[g] | | | | | | | | |
| | ~740–820[h] | | | | | | | | |
| | ~1170-1240[i] | | | | | | | | |

[a] In DMF;

[b] calculated as $\tau_{av} = \frac{\sum_{n=1}^{m} \alpha_n \tau_n^2}{\sum_{n=1}^{m} \alpha_n \tau_n}$;

[c] Shoulder-like relative maximum

[d] Hardly detectable;

[e] Main maximum in vibronically resolved signal.

[g] Uncharged film.

[h,i] Positively charged film.

consists in endowing it with active terminals based on heteroaromatic systems, like

(i) pyridine, a popular capping agent, also enabling to usefully exploit protonation equilibria and modulate electronic properties [38],

(ii) or (oligo)thiophene, particularly promoting radical-cation based coupling processes [39,40],

both of them also possibly contributing to global effective conjugation.

In this context, an insight is now proposed on the electrochemical features of the systematic series of cyclic triimidazole derivatives terminated with 4-pyridine, 2-thiophene and 2-bithiophene moieties reported in Scheme 2. An exhaustive voltammetry investigation, also integrated by (and in some cases combined with) absorption and emission spectroscopy and theoretical calculations, highlights the modulation of the electronic/redox properties and conjugation as a function of the terminal nature and multiplicity, also successfully testing the possibility to activate coupling/oligomerization processes, in the attractive perspective of electrochemically developing molecular materials endowed with **TT** functional properties combined with high electroactivity.

## 2. Synthesis of the TT derivatives

**BrTT, $Br_2$TT, $Br_3$TT**, **(4-Py)TT, $(4\text{-Py})_2$TT, $(4\text{-Py})_3$TT** and **(2-Th)$Me_2$Im** were prepared according to literature procedures [15,20,21,41].

**(2-Th)TT, $(2\text{-Th})_2$TT** and **$(2\text{-Th})_3$TT** were prepared by Stille coupling between 2-(tributylstannyl)thiophene and **BrTT, $Br_2$TT** and **$Br_3$TT** respectively (see Scheme 3 top; detailed protocols are reported in **SI1**).

**(2-biTh)TT, $(2\text{-biTh})_2$TT** and **$(2\text{-biTh})_3$TT** were prepared by Suzuki-Miyaura cross coupling between 2,2-bithiophene-5-boronic acid pinacol ester and **BrTT** or **$Br_2$TT** respectively (see Scheme 3 bottom; detailed protocols are reported in **SI1**).

## 3. Highlighting electron properties and electrochemical reactivity of the new TT families

The pyridine-, thiophene- and bithiophene- terminated **TT** series have been investigated by cyclic voltammetry CV at different scan rates, on glassy carbon GC working electrodes, in dimethylformamide, DMF and/or in some cases acetonitrile, $CH_3CN$, or/and dichloromethane, $CH_2Cl_2$, with 0.1 M tetrabutylammonium hexafluorophosphate, $TBAPF_6$, as supporting electrolyte; key results are summarized in Table 1. Support to result discussion and interpretation, particularly concerning electron energy levels and redox site localization, has been achieved by complementing the electrochemical investigation with absorption and emission electronic spectroscopy in $CH_2Cl_2$ and DMF at room temperature (detailed results in Table 2), as well as with theoretical modeling (**SI2**; detailed results in Table SI2.1). Results concerning LUMO and HOMO energy levels/gap estimation from the three approaches are also comparatively collected in Table 1. In particular, in the voltammetry case energy levels are estimated as follows:

$$E_{LUMO}(eV) \approx 1e \times \left(E_{p,Ic} \,/\, V(Fc^+|Fc) + 4.8V(Fc^+|Fc \; vs \; zero)\right]$$

$$E_{HOMO}(eV) \approx 1e \times \left(E_{p,Ia} \,/\, V(Fc^+|Fc) + 4.8V(Fc^+|Fc \; vs \; zero)\right]$$

a relationship widely employed in the literature, also consistent with a recent very accurate critical evaluation of $E_{O/R,\ CH3CN\ (SCE)} = E_{O/R,\ CH3CN\ (abs)} - 4.429$ V, $E_{O/R,DMF\ (SCE)} = E_{O/R,DMF\ (abs)} - 4.350$ V [42] combined with typical $E_{SCE}$ *vs* $Fc^+|Fc$ values of ~ 0.39 V in $CH_3CN$ or ~ 0.48 in DMF.

### 3.1. Electrochemistry and electronic properties of pyridine-terminated *TT* systems

As above mentioned, **TT** has little electrochemical activity, with first oxidation as well as first reduction only taking place close to the DMF potential window limits (about -3.2 V and 1.15 V vs $Fc^+|Fc$ respectively [33]).

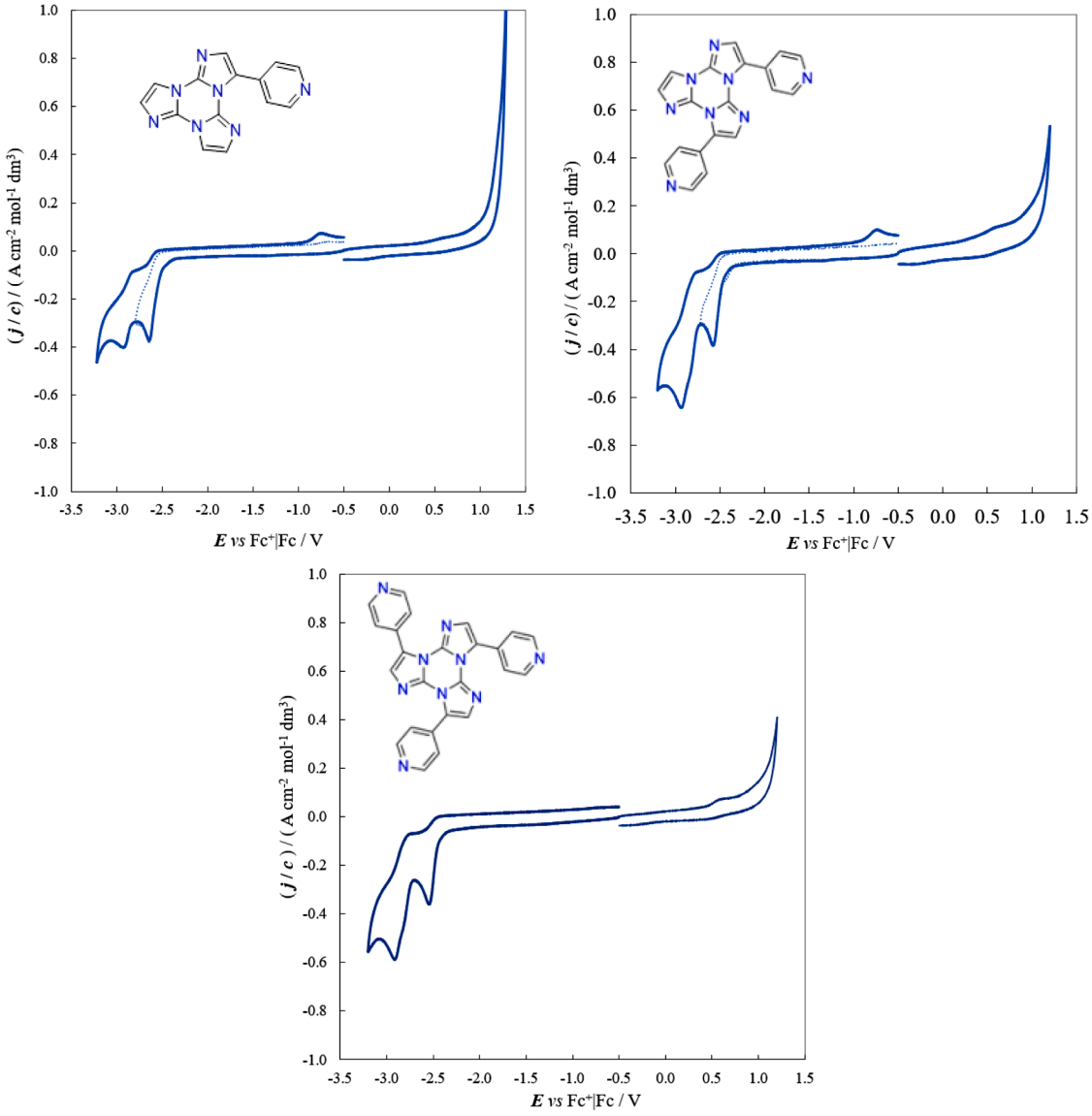


**Fig. 1.** A synopsis of normalized CV features for the **(4-Py)$_n$TT** systems at 0.2 V/s scan rate, on GC electrode, in DMF + 0.1 M $TBAPF_6$.

Although only slightly less extreme is the potential of pyridine first reduction to the corresponding radical anion (about -3.1 V [38]; actually, pyridine is often exploited as solvent rather than as reactant), **TT** functionalization with a pyridine unit significantly improves the molecule reactivity in the reduction region (Fig. 1).

It is useful to recall that in the cited parent work [33] a pyridine attached in ortho position to the **TT** system (**(2-Py)TT**, Scheme 1) resulted (i) on the reduction side, in a large positive shift of the first reduction potential to -2.8 V with a second reduction peak also becoming observable, as well as (ii) on the oxidation side, in a slight shift of the oxidation potential to a more favorable potential (1.07 V). Experiments at different scan rates pointed to **(2-Py)TT** first oxidation and first reduction being both electrochemically quasi reversible and chemically irreversible (although in the reduction case a return peak started to appear at high scan rates), while the second reduction peak appeared less kinetically facile, but also tending to chemical reversibility with increasing scan rate [33]. The first reduction peak was related to the formation of a radical anion with chemical follow up of moderate rate constant in competition with a second electron uptake at the second reduction peak, the latter resulting in formation of a dianion, possibly protonated to monoanion by trace water [33]. Considering the slightly easier reducibility of pyridine respect to **TT**, the first reduction site was assumed to be mostly localized on the 2-Py substituent, and the first oxidation one on the **TT** system [33].

Actually, since the electron attracting effect of pyridine as a substituent (accounted for by its Hammett constants, significantly positive in any case and much modulated by its linking position [40]) would in itself result in a significant positive shift of the **TT** CV features, looking at the slight negative shift of the first oxidation potential of **(2-Py)TT** with respect to **TT** it is evident that a conjugation effect prevailing over the inductive one should be considered between the **TT** core and the 2-Py pendant. In fact, increasing global conjugation efficiency promotes both first oxidation and first reduction processes, better stabilizing both the resulting radical cations and radical anions. Indeed, theoretical computations with related orbital plots now confirm the formerly assumed partial involvement of the Py terminal in the mostly **TT**-centered HOMO orbital as well as the partial **TT** involvement in the mostly Py-centered LUMO orbital (Fig. 2, Table SI2.1).

Notably, a remarkable positive shift of both reduction and oxidation processes is observed by attaching the pyridine substituent by its *p*- rather than *o*- position (**(4-Py)TT** *vs* **(2-Py)TT**) to the **TT** core, resulting in a first reduction peak more positive by about 0.16 V (Table 1,

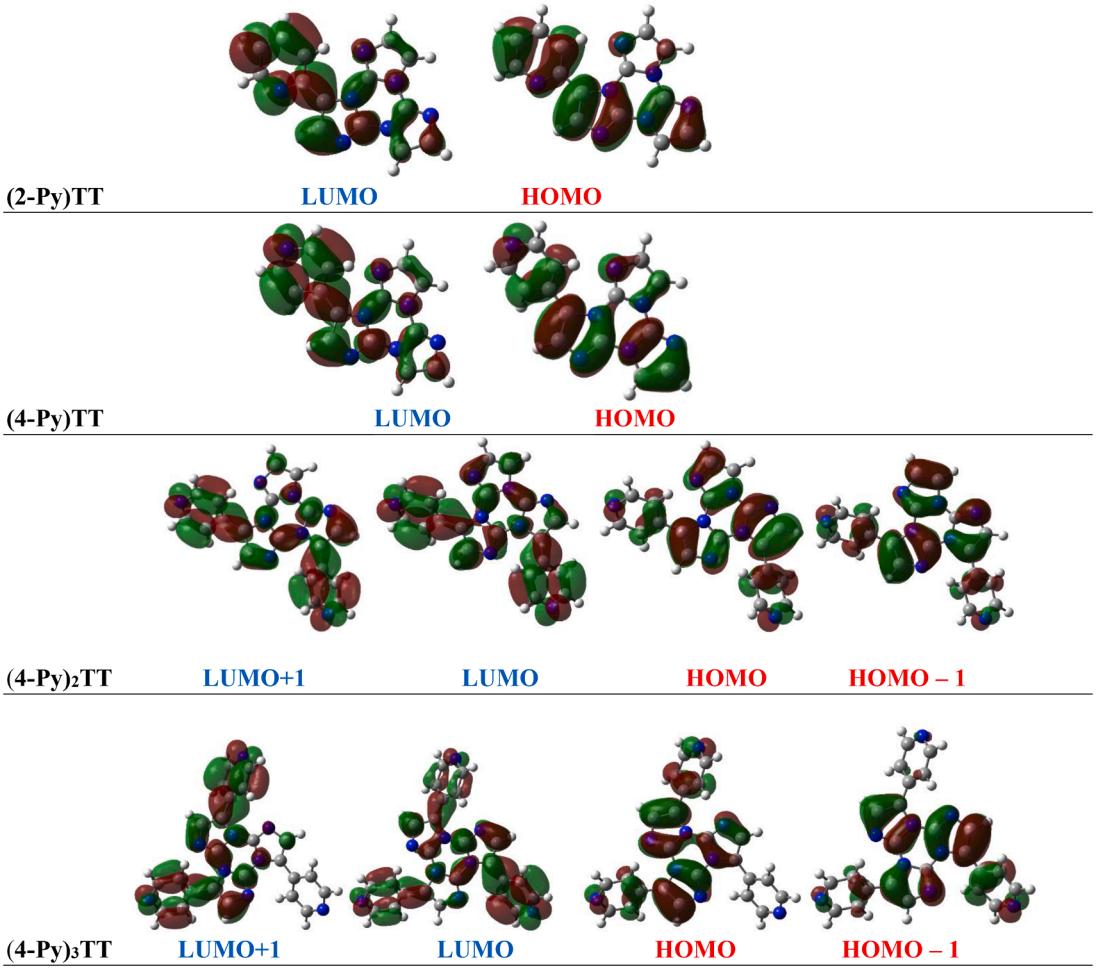


**Fig. 2.** DFT plots of orbitals mainly involved in the lower energy transitions for the **(2-Py)TT and (4-Py)$_n$TT** systems (isosurface value 0.02).

consistent with the calculated $E_{LUMO}$ shift of about 0.11 eV, Table S3), and the oxidation peak displaced beyond the DMF window positive limit (consistent with the calculated $E_{HOMO}$ shift of about 0.35 eV, Table S3). Now, substituent inductive effects on the reactivity of aromatic molecules are usually similar for *o*- and *p*- positions, but specific effects can result in anomalies for the *o*- position; actually Hammett constants are only provided for substituents attached in *p*- and *m*- positions, $\sigma_p$ and $\sigma_m$ respectively [43]. In the case of pyridine, a remarkable difference in the reactivity of the N position upon *o*- *vs p*- functionalization with the same substituent has been long observed. For example, in a classical work [44], the much higher impact is highlighted of *o*- substituents on the N doublet availability, justified considering a local electrostatic effect rapidly fading with distance [44], which is consistent with the pyridine N doublet being not included in the aromatic system, unlike *e.g.* the pyrrole case. Specularly, the $\sigma_p$ Hammett constants for pyridine regarded as a substituent remarkably depend on its linking position, steeply increasing with increasing distance from the N position ($\sigma_p$ = 0.17/0.25/0.44 with 2-pyridyl, 3-pyridyl and 4-pyridyl substituents, respectively [43]); thus a 4-pyridyl substituent is much more electron attracting than a 2-pyridyl one.

Notably, the effect of the linking position of pyridyl groups is more conspicuous in the case of HOMO and oxidation, a mostly **TT**-centered process, than in the case of LUMO and reduction, a mostly pyridine-centered process (Fig. 2), as it is evident according to both DFT calculations and CV results comparing **(4-Py)TT** and **(2-Py)TT** data in Table 1. As a result, the HOMO-LUMO gap, while dramatically decreasing for both derivatives with respect to parent **TT**, is significantly smaller for **(2-Py)TT** than **(4-Py)TT**.

Increasing the number of Py terminals (from **(4-Py)TT** to **(4-Py)$_2$TT** and **(4-Py)$_3$TT**) the first reduction peak remains remarkably similar not only in features (electrochemically quasi reversible, chemically irreversible) but also in height, suggesting that it might still correspond to a single reduction process, although increasingly favored since the peak potential slightly shifts to less negative values with increasing the number of pyridine substituents (-2.64/-2.60/-2.54 V for n = 1/2/3). This trend is also consistent with the trend of DFT calculated values for the LUMO orbitals, and can be justified by the increased effective conjugation, both pyridine groups being involved in LUMO as well as LUMO+1. At the same time an additional reduction peak appears, nearly superimposed on the quasi reversible second reduction peak. This could be justified in terms of radical anion formation on a second nearly equivalent, strongly interacting redox centre (considering the ~0.2 V potential difference). Notably, the CV pattern is practically the same for **(4-Py)$_2$TT** and **(4-Py)$_3$TT**, that is, the presence of the third pyridine site has apparently no effect in the available potential window, excepting for the slight positive shift of the first reduction potential, linked to the slight increase of effective conjugation (consistently with a negligible involvement of the third pyridine ring in the LUMO according to the DFT electron density map, Fig. 2).

Consistently with the electrochemical activity, also the intrinsically very poor electronic spectroscopy behavior of **TT** is significantly improved upon functionalization with one or more pyridine groups, in terms of both absorption and emission properties. Solutions of parent **TT** are characterized by very small oscillator strengths for the low energy transitions, due to the high symmetry of the molecule; this results in poorly emissive features and a very weak absorption at 285 nm with a

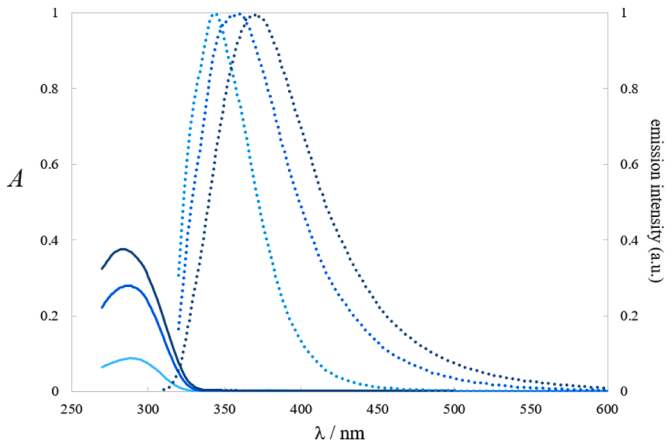


**Fig. 3.** UV-vis absorption and emission (solid and dotted lines, respectively) for the **(4-Py)$_n$TT** systems ($n$ = 1,2,3 for light/medium/dark blue, respectively) $10^{-5}$ M in DMF.

first sizable peak at about 220 nm (Fig. S17).

Functionalization with one or more pyridine terminals results in significant enhancement of both absorption and emission activity. Consistently with the availability of the pyridine-centered much lower LUMO, the first absorption process can take place at a significantly lower energy. Notably, upon increasing the number of pyridine terminals such absorption peak is located at nearly constant maximum wavelength while its molar extinction coefficient increases (Table 2, Figs. 3 and S18), which would point to only partial electronic communication among the pyridine terminals.

It is worthwhile noticing that, according to the above observations, the pyridine terminals look more independent when investigated as equivalent chromophores in UV-Vis spectroscopy than when investigated as equivalent redox sites in voltammetry. However, different processes are involved in the two experiments: in the first case, electron transitions within the molecule depending on HOMO-LUMO gaps with no net charge(s) formation in a pure solvent; in the second case, electron transfers to the molecule, depending on its LUMO energy only, and resulting in net charge(s) formation in the solvent added with a supporting electrolyte. Moreover, it could be questioned whether the large first UV-Vis absorption peak might actually account for the merging of

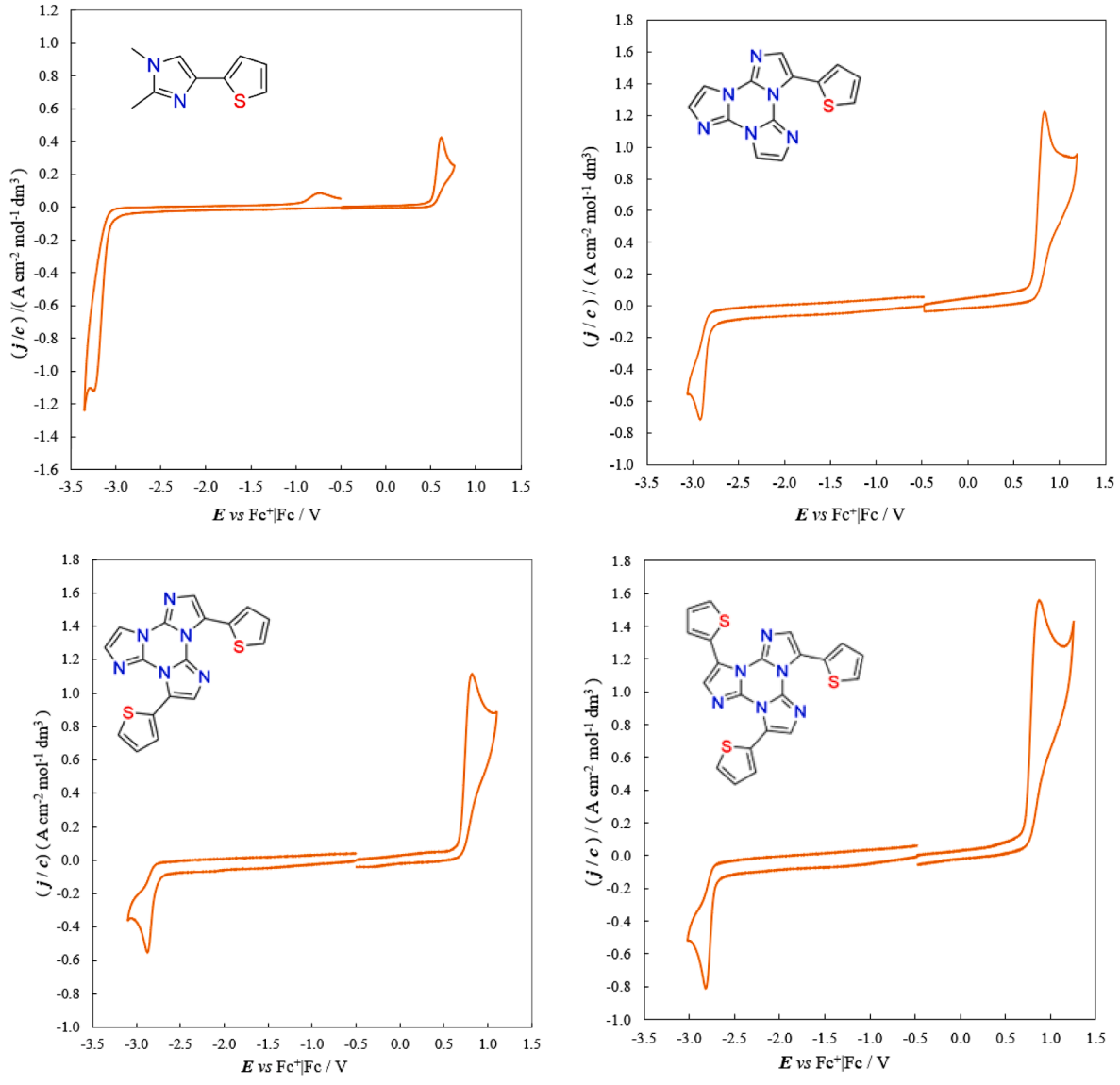


**Fig. 4.** A synopsis of normalized CV features for the **(2-Th)$_n$TT** systems and for model **(2-Th)Me$_2$Im**, at 0.2 V/s scan rate, on GC electrode, in DMF + 0.1 M $TBAPF_6$.

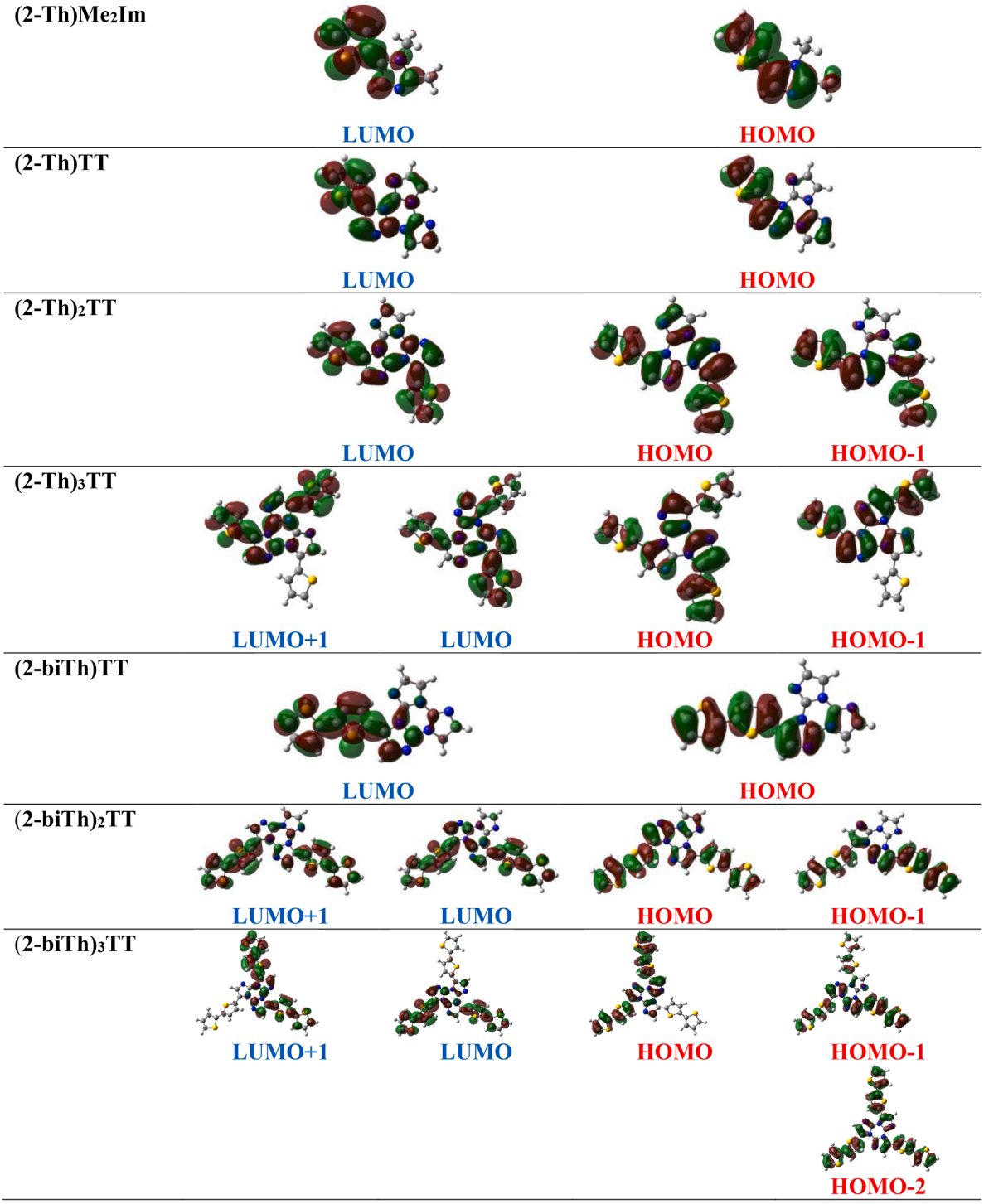


**Fig. 5.** DFT plots of orbitals mainly involved in lower energy transitions for the **(2-Th)$_n$TT** and **(2-biTh)$_n$TT** systems with related model molecule **(2-Th)Me$_2$Im** (isosurface value 0.02).

1/2/3 processes at slightly decreasing wavelengths, which would be also consistent with the regularly decreasing trend of the maximum wavelength with increasing number of pyridine terminals. An analogy could be found in the case of chiral molecules with axial stereogenicity, featuring two moieties that are at the same time two equivalent redox sites and two equivalent chromophores: voltammetry is usually able to highlight their interaction resulting in twin peak systems, while a single wide absorption peak is usually observed in achiral UV-Vis spectroscopy; however, in circular dichroism spectroscopy a typical sigmoidal signature can be observed, evidencing that a significant difference actually exists in absorption wavelengths for the interacting chromophores [45].

Concerning emission properties, one broad fluorescence, with significant quantum yields (Φ≅ 25%, Table 2) is observed for $10^{-5}$ M solutions of **(4-Py)TT, (4-Py)$_2$TT** and **(4-Py)$_3$TT**, both in DMF and $CH_2Cl_2$, with maximum wavelength at 356/393/401 nm and 345/359/371 nm, respectively (Table 2, Figs. 3 and S19). Notably, differently from absorption, the effect of the number of pyridine terminals on the emission wavelength is quite perceivable, resulting in both solvents in an increasing Stokes shift along the series (Table 2, Fig. 3). This observation

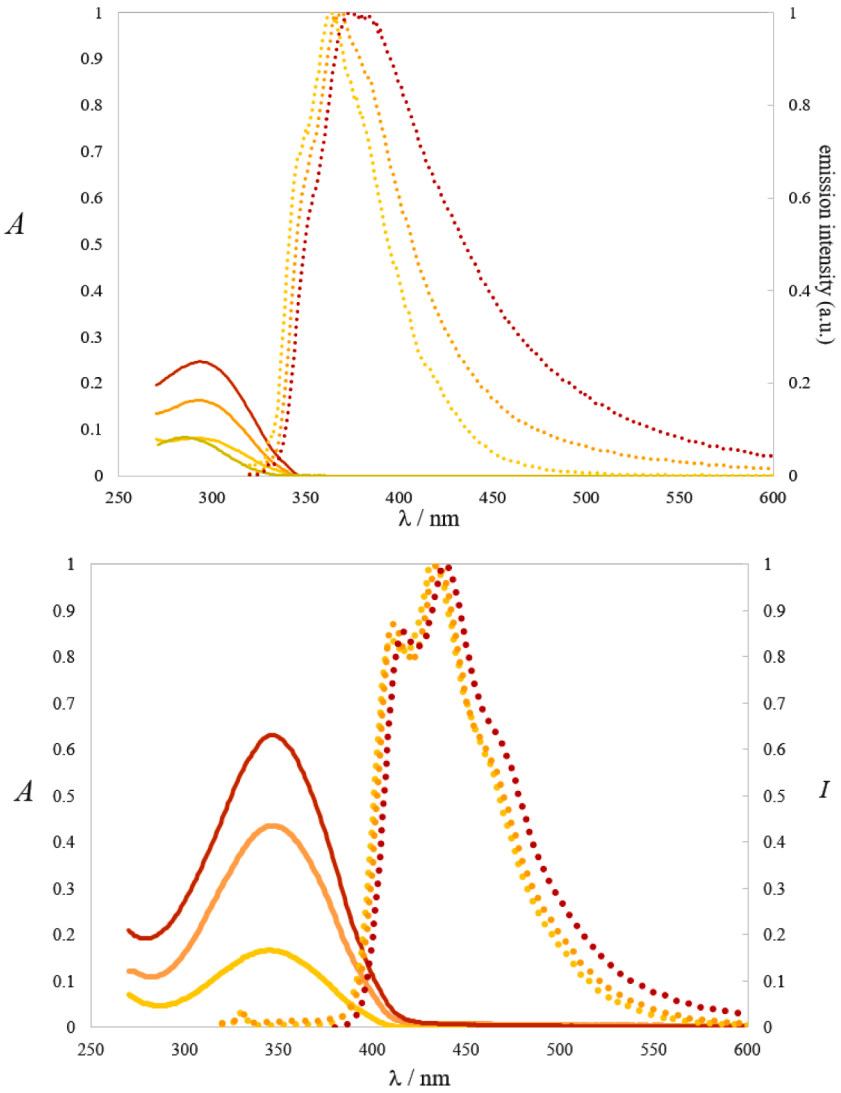


**Fig. 6.** Top: UV-vis absorption and emission (solid and dotted thin lines, respectively) for the **(2-Th)$_n$TT** systems $10^{-5}$ M in DMF (n = 1,2,3 for light/medium/dark orange, respectively). Bottom: UV-vis absorption and emission (solid and dotted thick lines, respectively) for the **(2-biTh)$_n$TT** systems $10^{-5}$ M in DMF ($n$ = 1,2,3 for light/medium/dark orange, respectively).

might be related to an increase in excited state conformational freedom with increasing number of terminal substituents [46,47].

The small but significant solvatochromic effects (higher wavelengths being observed for both absorption and emission features increasing the solvent polarity, Table 2) look consistent with the significant change of localization between HOMO and LUMO orbitals (Fig. 2), which is also accounted for by the significant changes in the computed ground and excited states dipole moments.

### 3.2. *Electrochemistry and electronic properties of thiophene- and bithiophene-terminated **TT** systems*

Substitution of the **TT** scaffold with one or more thiophene groups (**(2-Th)TT, (2-Th)$_2$TT, (2-Th)$_3$TT**) results in much milder potentials for both first oxidation and first reduction, both of them well perceivable in the available potential window (Fig. 4), implying a lower LUMO, a higher HOMO and a narrower HOMO-LUMO gap with respect to parent **TT**, which is also consistent with calculations and UV-vis absorption data (Tables 1 and 2).

In accordance with thiophene features (electron rich ring, with the S atom included in the aromatic system, and with very small Hammett parameters, *i.e.* $\sigma_m$=0.09 or $\sigma_p$=0.05 if linked in position 2 [43], with respect to the strong electron attracting character of pyridine), the thiophene-substituted series looks not only significantly electron richer than the pyridine-substituted one, but also with a more effective improvement of global conjugation efficiency, since the potential shifts of first oxidation and first reduction to milder values are comparable, and the inductive effect of thiophene is small.

DFT calculations do confirm that thiophene terminals are significantly involved in both HOMOs and LUMOs (Fig. 5). Consistently, both DFT-calculated and spectroscopically observed HOMO-LUMO gaps are slightly but significantly narrower for the **(2-Th)$_n$TT** compounds with respect to their **(2-Py)$_n$TT** analogues (Tables 1 and 2). Actually, concerning spectroscopic features, the two series share many analogies together with some differences. In particular, when working in the same solvent and at the same concentration, the first absorption maxima wavelengths of **(2-Th)$_n$TT** compounds are similar and even less affected by the active terminal number than in the **(2-Py)$_n$TT** case, while their molar extinction coefficients are somehow lower but still regularly increasing with the number of active terminals (Fig. 6 top). In emission all **(2-Th)$_n$TT** derivatives also show one broad fluorescence (Fig. 6 top) with quantum yields significantly lower than those of **(2-Py)$_n$TT**, although still sizable ($\Phi \cong$ 9 %) (Table 2). The Stokes shifts are comparable, and show the same trend with increasing terminal number,

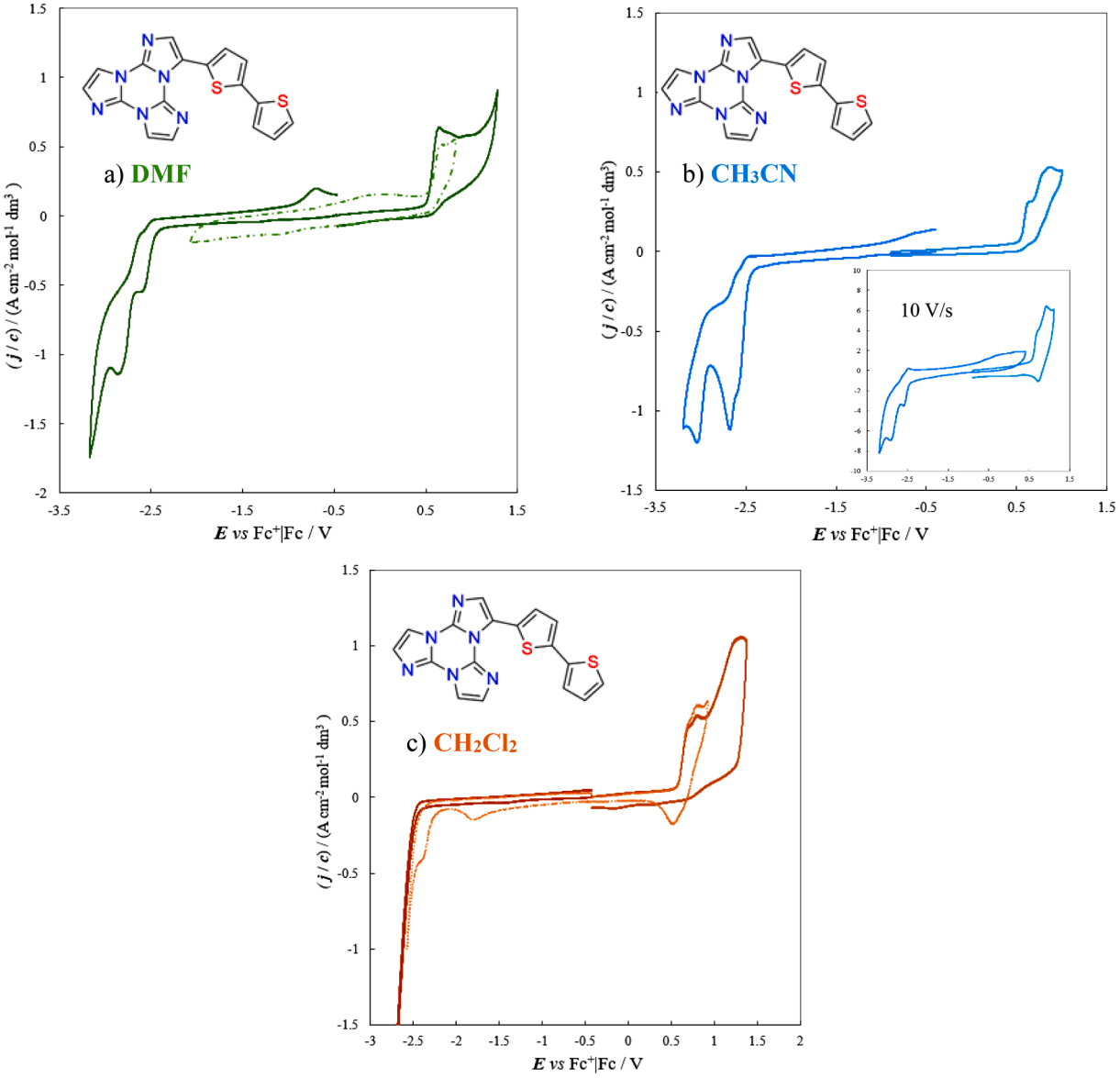


**Fig. 7.** A synopsis of normalized CV features at 0.2 V/s on GC electrode for **(2-biTh)TT**, in DMF (a), or $CH_3CN$ (b) or $CH_2Cl_2$ (c), all of them with 0.1 M $TBAPF_6$ supporting electrolyte.

supporting the above assumption of an increasingly higher excited state conformational freedom. Similar solvatochromic effects are also observed in both absorption and emission (Table 2).

The significant contribution of the **TT** core, albeit of little intrinsic activity, to the overall conjugation is highlighted by comparing the CV features of **(2-Th)TT** with the **(2-Th)$Me_2$Im** model (Fig. 4). In fact, in the latter case both first oxidation and first reduction are displaced to more negative values by 200–300 mV and the gap is larger by about 100 mV; such feature combination can be justified considering, together with the electron donating inductive effect of the two methyl groups, a significant decrease in global conjugation upon changing the cyclic triazole unit with a simple imidazole group.

Both first oxidation and first reduction of **(2-Th)$_n$TT** are chemically irreversible in the experimental potential scan rate range. At the same time, the small potential shift with scan rate points to rather fast electron transfer processes, especially concerning first reduction, in which case the half-peak width is close to the 57 mV expected value for a mono-electronic process. In comparison the first oxidation peak is much larger and about twice higher, pointing to a more complex process.

Actually, an additional bonus provided by thiophene terminals is the possibility of coupling reactions by electrochemical generation of radical cations [39,40]. However, we did not observe significant formation of an electroactive film on the electrode surface when testing the thiophene-terminated series in DMF at concentrations of the order of $10^{-3}$ M, nor was successful a test in a less polar solvent like $CH_2Cl_2$ with the fully functionalized **(2-Th)$_3$TT** (Fig. SI.33), the most promising candidate in the series for coupling events on account of the abundance of active terminals around the **TT** core.

Assuming that the thiophene terminals are too small in comparison with the bulkiness of the **TT** core, and that more freedom degrees would more efficiently promote coupling and network formation, we prepared and tested *bi*thiophene derivatives **(2-biTh)TT, (2-biTh)$_2$TT** and **(2-biTh)$_3$TT**. For all of them first oxidation takes place at much lower potentials than their thiophene homologues, by about 0.2 V (Figs. 7 and 8, Table 1). This is consistent with the HOMO chiefly involving the bithiophene group (Fig. 5), but also benefiting of a global higher conjugation with respect to benchmark α-bithiophene (Table 1). Significant, although smaller, is also the shift of the first reduction peak to less negative values; actually also the LUMO looks mainly located on the bithiophene group (Fig. 5); as a result, the energy gap is much smaller

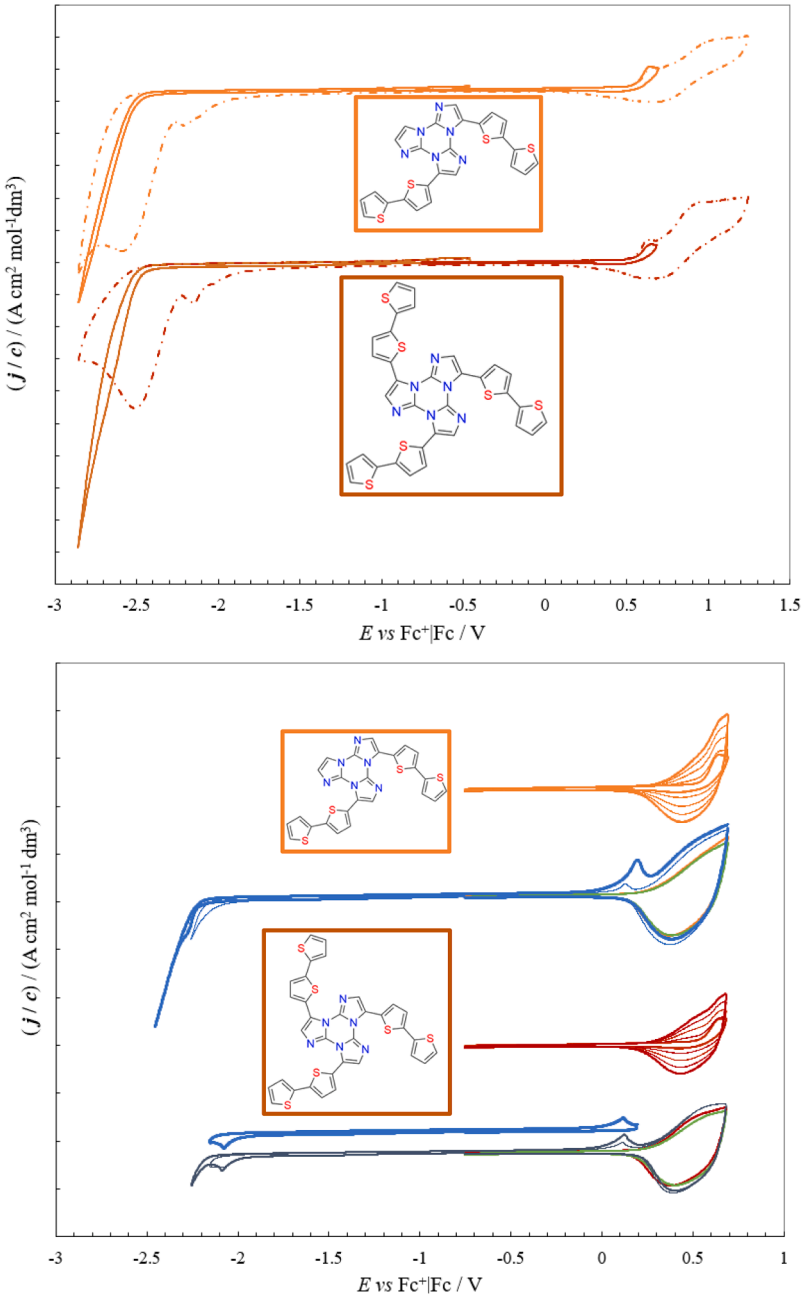


**Fig. 8.** Comparative synopses of normalized CV features on GC electrode for **(2-biTh)$_2$TT** and **(2-biTh)$_3$TT** with the same operating protocols, in $CH_2Cl_2$ with 0.1 M $TBAPF_6$ supporting electrolyte. Top: monomer CV features at 0.2 V/s. Bottom: potentiodynamic electrooligomerizations at 0.2 V/s scan rate (with I, III, VI, IX, XII cycles reported), followed by stability cycles in monomer-free solution (V cycle reported in green over the last deposition cycle) and by potential cycle widening towards more negative potentials enabling to highlight charge trapping effects (reported in blue).

(Tables 1, **SI2.1**). This is also in accordance with spectroscopic features (Fig. 6 bottom *vs* Fig. 6 top, Tables 1 and 2). Absorption wavelengths are red-shifted by about 50 nm and again nearly independent on the terminal number, while molar extinction coefficients again increase with it; moreover, they are 2 - 3 times higher than in the thiophene series. Concerning emission, the **(2-biTh)$_n$TT** molecules exhibit a broad fluorescence band and Stokes shifts similar to those of the monothiophene analogues.

Looking for a solvent promoting electrodeposition of an electroactive coupling product, the monosubstituted derivative **(2-biTh)TT** was investigated in other solvents beside DMF (Fig. 7a), *i.e.* $CH_3CN$ (Fig. 7b) and $CH_2Cl_2$ (Fig. 7c). Intriguingly, both first oxidation in $CH_3CN$ and $CH_2Cl_2$ as well as first reduction in DMF and $CH_3CN$ (while not observable in $CH_2Cl_2$ on account of the smaller potential window on the reduction side) look as twin peak systems, nearly merging in the oxidation case, increasingly with increasing scan rate, as in the case of equivalent or nearly equivalent interacting redox sites.

In $CH_2Cl_2$ first oxidation of **(2-biTh)TT** results in the formation of an electroactive product on the electrode surface (while only weak hints could be perceived in DMF and $CH_3CN$), revealed by the reproducible appearance, at any scan rate, of two reduction processes subsequent to first oxidation (Fig. 7c, dash-and-dot line). Such CV pattern however provides no evidence of active film growth since it remains the same upon repeated cycling, with no change in the first oxidation peak system. This could be justified in terms of bithiophene radical cation coupling resulting in reproducible formation of a dimer layer on the electrode surface, which is actually the only coupling process available for monofunctionalized **(2-biTh)TT**; in this case the reduction peaks might correspond to radical anion and dianion formation. In any case, such product layer does not accumulate, looking unstable and/or readily soluble, and it has been no further explored.

Instead di- and trisubstituted monomers **(2-biTh)$_n$TT** (n = 2, 3) in $CH_2Cl_2$, although exhibiting CV features quite similar to their monosubstituted analogue **(2-biTh)TT** with only very slight shifts of the

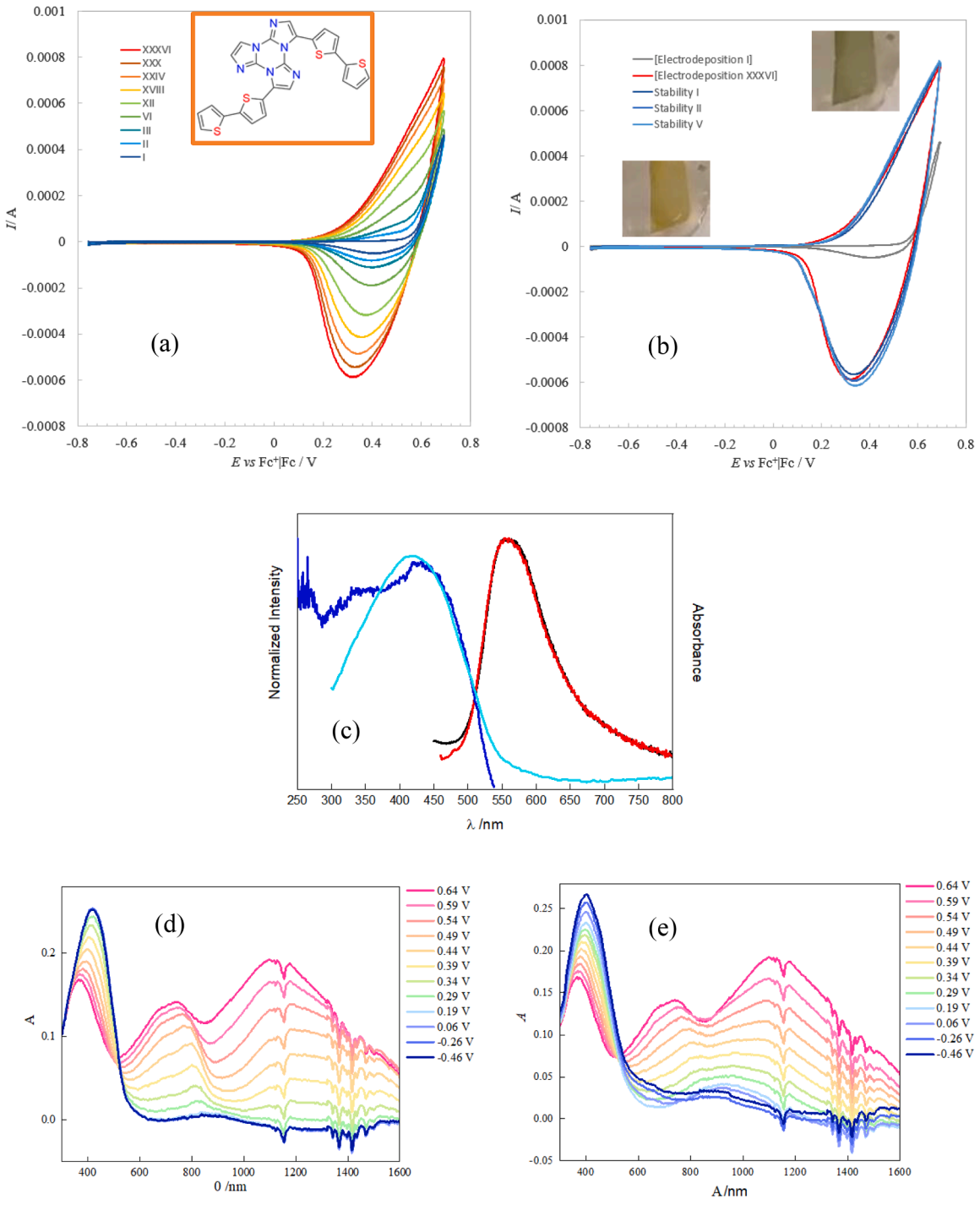


**Fig. 9.** Spectroscopic and spectroelectrochemical features of **[(2-BiTh)$_2$TT]$_n$** films electrochemically formed on ITO electrode. (a) Potentiodynamic electrodeposition in ~0.0009 M monomer solution in $CH_2Cl_2$ + 0.1 M $TBAPF_6$, (36 cycles at 0.2 V/s, selected cycles reported); (b) Selected stability cycles in monomer-free solution, and electrochromism; (c) A synopsis of UV-Vis absorption (cyan line), excitation ($\lambda_{em}$ 558 nm blue line) and emission ($\lambda_{exc}$ 350 nm black line; $\lambda_{exc}$ 446 nm red line); spectra of the film in uncharged state. (d,e) UV-Vis /NIR spectra for a film deposited with the same protocol, polarized at increasing (d) and subsequently decreasing (e) potentials, referred to $Fc^+|Fc$ in $CH_2Cl_2$ + 0.1 M $TBAPF_6$.

oxidation and reduction potentials to milder values, have quite different outcomes for the first oxidation process, *i.e.* fast and regular growth of electroactive films on the electrode surface upon potential cycling around the first oxidation peak, both on GC electrode (Figs. 8, S34) and on ultraflat ITO electrode (Figs. 9 and 10).

**[(2-biTh)$_2$TT]$_n$** films thus obtained are stable upon potential cycling in monomer-free solution (Fig. 8), electrochromic (Fig. 9), with charge trapping effects depending on operating conditions (Fig. 8). They have high conjugation efficiency (their estimated HOMO-LUMO gap being ~2.85 eV from their UV-Vis maximum wavelengths or ~2.2 eV from onset wavelengths), and are highly electroactive. They exhibit oxidation onsets comparable to, and even less positive than, benchmark α-tetrathiophene (Table 1); moreover, their EIS patterns (Figs. S34, S35), consistent with "finite reflexive diffusion" conditions [48], show that the film positive charging is kinetically very facile. In fact, charge transfer resistance $R_{CT}$ (accounting for the electron transfer activation barrier) is

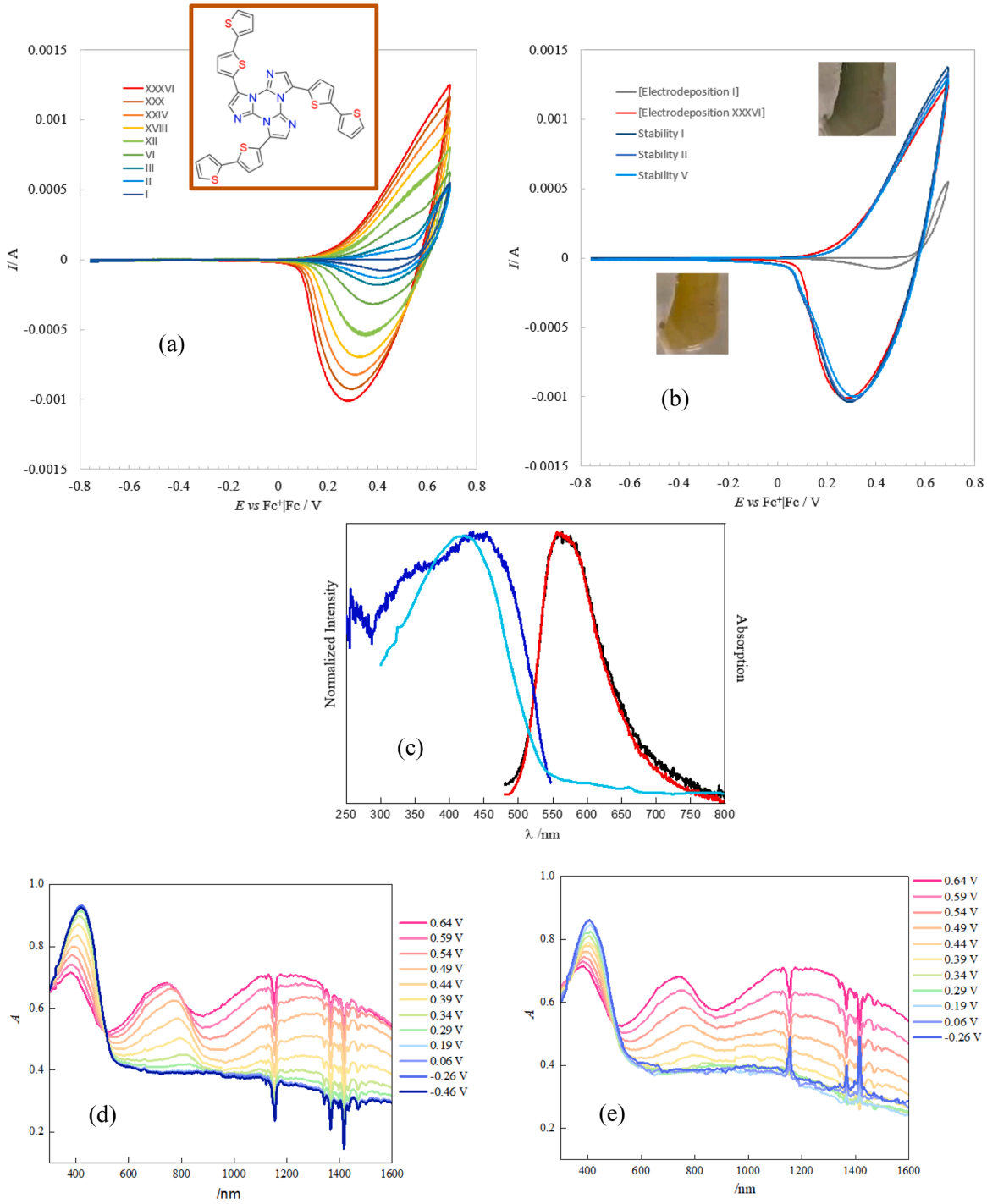


**Fig. 10.** Spectroscopic and spectroelectrochemical features of **[(2-BiTh)$_3$TT]$_n$** films electrochemically formed on ITO electrode. (a) Potentiodynamic electrodeposition in ~0.0008 M monomer solution in $CH_2Cl_2$ + 0.1 M $TBAPF_6$, (36 cycles at 0.2 V/s, selected cycles reported); (b) Selected stability cycles in monomer-free solution, and electrochromism; (c) A synopsis of UV-Vis absorption (cyan line), excitation ($\lambda_{em}$ 567 nm blue line) and emission ($\lambda_{exc}$ 350 nm black line; $\lambda_{exc}$ 446 nm red line) spectra of the film in uncharged state. (d,e) UV-Vis /NIR spectra for a film deposited with the same protocol, polarized at increasing (d) and subsequently decreasing (e) potentials, referred to $Fc^+|Fc$ in $CH_2Cl_2$ + 0.1 M $TBAPF_6$.

nearly unperceivable and/or disappears soon after the oxidation onset. Moreover, the Warburg behavior is nearly unperceivable, pointing to easy uptake of balancing counteranions within the film, and charge saturation, accounted for by the quasi capacitive behavior at low frequencies, is reached very early.

The electrochromic features of films electrodeposited on ultraflat ITO electrodes have been also highlighted in more detail by spectroelectrochemistry experiments (Figs. 9 and 10, S36). With increasingly positive charging of the film, the neutral film absorption peak decreases with concurrent increase of two larger absorption bands at ~700–800 and ~1100–1200 nm (Figs. 9d and 10d, S36d). Consistently with polythiophene properties, the two absorption peaks of the charged film should correspond to radical cation (polaron) and dication (dipolaron) formation, resulting in improved planarity and therefore conjugation efficiency. With the film deposition protocol adopted in the experiments in Figs. 9 and 10, the trend of the absorption spectra appears nearly

reversible in the backward potential steps (Figs. 9d and 10d).

The films exhibit a broad fluorescence peak (Figs. 9c and 10c, S36c) which is strongly quenched through charging process (Fig. S25).

According to these preliminary results, most features in the oligomerization processes and in the obtained films strongly resemble oligothiophene ones, which is quite reasonable considering the above discussion of the electronic properties in the **(2-biTh)$_n$TT** series (and the very role of the purposedly introduced bithiophene terminals). We look forward to investigating the morphological features and chemical/functional properties of the new **TT**-tetrathiophene films in more detail, with a wider range of operating conditions and characterization techniques; particularly attractive targets are both *(i)* to highlight role and functional properties of the **TT** modules in the **TT**-tetrathiophene materials, and *(ii)* to highlight, exploiting the **(2-biTh)$_n$TT** series as a very convenient topological study case, the difference between films obtained from the disubstituted monomer, enabling chain-like propagation, *vs* those obtained in the same conditions from the trisubstituted monomer, which could also enable network-like propagation.

## 4. Conclusions

Cyclic triimidazole **TT**, a multipurpose molecular tool with an attractive range of advanced potential applications, can have its functional properties modulated, enhanced, or/and even transferred into **TT**-based molecular materials, by functionalization with appropriate heteroaromatic terminals, like pyridine, a popular protonable capping agent, or thiophene/bithiophene ones, promoting coupling processes.

The present exhaustive voltammetry investigation, integrated by electronic spectroscopies and supported by theoretical calculations, effectively highlights the enhancement in electrochemical and spectroscopic activity as a function of the nature and number of the active terminals. Such observations provide important guidelines for future design and exploitation of advanced **TT** derivatives.

Moreover, two first examples are presented of electrochemically and spectroscopically highly active oligo/polymer films based on alternated **TT** and tetrathiophene units, that can be obtained by fast and reproducible oxidative electrodeposition from a **TT** derivative with two or three bithiophene terminals.

We look forward to carrying out a more detailed investigation of the new **TT**-tetrathiophene materials, particularly aiming to highlight role and functional properties of the **TT** units as well as to highlight the difference between films obtained from the disubstituted monomer, enabling chain-like propagation, *vs* those obtained in the same conditions from the trisubstituted monomer, which could also enable network-like propagation: indeed a very nice topological study case.

In any case, the present preliminary results can be regarded as an attractive starting point in the perspective of electrochemically developing molecular materials endowed with **TT** functional properties combined with high electroactivity.

## CRediT authorship contribution statement

**Daniele Malpicci:** Investigation, Data curation, Writing – review & editing. **Silvia Rosa Araneo:** Investigation, Writing – review & editing. **Serena Arnaboldi:** Investigation, Data curation. **Elena Cariati:** Conceptualization, Supervision, Writing – review & editing. **Alessandra Forni:** Investigation, Data curation. **Sara Grecchi:** Investigation, Data curation. **Elena Lucenti:** Investigation, Data curation, Writing – original draft. **Daniele Marinotto:** Investigation, Data curation. **Daniele Maver:** Investigation, Data curation. **Patrizia Romana Mussini:** Conceptualization, Investigation, Data curation, Supervision, Writing – original draft.

## Declaration of Competing Interest

The authors declare that they have no known competing financial interests or personal relationships that could have appeared to influence the work reported in this paper.

## Data availability

Data will be made available on request.

## Acknowledgments

The use of instrumentation purchased through the SmartMatLab Project (cofunded by Fondazione Cariplo, Regione Lombardia and Università degli Studi di Milano) is gratefully acknowledged, as well as support from Fondazione Cariplo and Regione Lombardia (2016-0923).

## Supplementary materials

Supplementary material associated with this article can be found, in the online version, at doi:10.1016/j.electacta.2023.143117.

## References

[1] Q. Dang, Y. Jiang, J. Wang, J. Wang, Q. Zhang, M. Zhang, S. Luo, Y. Xie, K. Pu, Q. Li, Z. Li, Room-temperature phosphorescence resonance energy transfer for construction of near-infrared afterglow imaging agents, Adv. Mater. 32 (2020), 2006752.

[2] Y. Wang, H. Gao, J. Yang, M. Fang, D. Ding, B.Z. Tang, Z. Li, High performance of simple organic phosphorescence host–guest materials and their application in time-resolved bioimaging, Adv. Mater. 33 (2021), 2007811.

[3] W. Qin, P. Zhang, H. Li, J.W.Y. Lam, Y. Cai, R.T.K. Kwok, J. Qian, W. Zheng, B. Z. Tang, Ultrabright red AIEgens for two-photon vascular imaging with high resolution and deep penetration, Chem. Sci. 9 (2018) 2705–2710.

[4] J. Zhi, Q. Zhou, H. Shi, Z. An, W. Huang, Organic room temperature phosphorescence materials for biomedical applications, Chem. Asian J. 15 (2020) 947–957.

[5] L. Gu, H. Wu, H. Ma, W. Ye, W. Jia, H. Wang, H. Chen, N. Zhang, D. Wang, C. Qian, Z. An, W. Huang, Y. Zhao, Color-tunable ultralong organic room temperature phosphorescence from a multicomponent copolymer, Nat. Commun. 11 (2020) 944.

[6] Y. Lei, W. Dai, J. Guan, S. Guo, F. Ren, Y. Zhou, J. Shi, B. Tong, Z. Cai, J. Zheng, Y. Dong, Wide-range color-tunable organic phosphorescence materials for printable and writable security inks, Angew. Chem. Int. Ed. 59 (2020) 16054–16060.

[7] J. Tan, Q. Li, S. Meng, Y. Li, J. Yang, Y. Ye, Z. Tang, S. Qu, X. Ren, Time-Dependent phosphorescence colors from carbon dots for advanced dynamic information encryption, Adv. Mater. 33 (2021), 2006781.

[8] S. Hirata, Recent advances in materials with room-temperature phosphorescence: photophysics for triplet exciton stabilization, Adv. Opt. Mater. 5 (2017), 1700116.

[9] Z. An, C. Zheng, Y. Tao, R. Chen, H. Shi, T. Chen, Z. Wang, H. Li, R. Deng, X. Liu, W. Huang, Stabilizing triplet excited states for ultralong organic phosphorescence, Nat. Mater. 14 (2015) 685–690.

[10] X. Zhen, Y. Tao, Z. An, P. Chen, C. Xu, R. Chen, W. Huang, K. Pu, Ultralong phosphorescence of water-soluble organic nanoparticles for *in vivo* afterglow imaging, Adv. Mater. 29 (2017), 1606665.

[11] L. Gu, H. Shi, C. Miao, Q. Wu, Z. Cheng, S. Cai, M. Gu, C. Ma, W. Yao, Y. Gao, Z. An, W. Huang, Prolonging the lifetime of ultralong organic phosphorescence through dihydrogen bonding, J. Mater. Chem. C 6 (2018) 226–233.

[12] S. Cai, H. Shi, D. Tian, H. Ma, Z. Cheng, Q. Wu, M. Gu, L. Huang, Z. An, Q. Peng, W. Huang, Enhancing ultralong organic phosphorescence by effective π-type halogen bonding, Adv. Funct. Mater. 28 (2018), 1705045.

[13] J. Wang, B. Liang, J. Wei, Z. Li, Y. Xu, T. Yang, C. Li, Y. Wang, Highly efficient electrofluorescence material based on pure organic phosphor sensitization, Angew. Chem. Int. Ed. 60 (2021) 15335–15339.

[14] E. Lucenti, A. Forni, C. Botta, L. Carlucci, C. Giannini, D. Marinotto, A. Previtali, S. Righetto, E. Cariati, H-aggregates granting crystallization-induced emissive behavior and ultralong phosphorescence from a pure organic molecule, J. Phys. Chem. Lett. 8 (2017) 1894–1898, https://doi.org/10.1021/acs.jpclett.7b00503.

[15] E. Lucenti, A. Forni, C. Botta, L. Carlucci, C. Giannini, D. Marinotto, A. Pavanello, A. Previtali, S. Righetto, E. Cariati, Cyclic triimidazole derivatives: intriguing examples of multiple emissions and ultralong phosphorescence at room temperature, Angew. Chem. Int. Ed. 56 (2017) 16302–16307, https://doi.org/10.1002/anie.201710279.

[16] E. Lucenti, E. Cariati, A. Previtali, D. Marinotto, A. Forni, V. Bold, V.C. Kravtsov, M. S. Fonari, S. Galli, L. Carlucci, Versatility of cyclic triimidazole to assemble 1D, 2D, and 3D Cu(I) halide coordination networks, Cryst. Growth Des. 19 (2019) 1567–1575, https://doi.org/10.1021/acs.cgd.8b01199.

[17] M.S. Fonari, V.C. Kravtsov, V. Bold, E. Lucenti, E. Cariati, D. Marinotto, A. Forni, Structural landscape of Zn(II) and Cd(II) coordination compounds with two isomeric triimidazole luminophores: impact of crystal packing patterns on emission

properties, Cryst. Growth Des. 21 (2021) 4184–4200, https://doi.org/10.1021/acs.cgd.1c00459.
[18] D. Malpicci, E. Lucenti, A. Forni, D. Marinotto, A. Previtali, L. Carlucci, P. Mercandelli, C. Botta, S. Righetto, E. Cariati, Ag(I) and Cu(I) cyclic-triimidazole coordination polymers: Revealing different deactivation channels for multiple room temperature phosphorescences, Inorg. Chem. Front. 8 (2021) 1312–1323, https://doi.org/10.1039/d0qi01377c.
[19] A. Previtali, W. He, A. Forni, D. Malpicci, E. Lucenti, D. Marinotto, L. Carlucci, P. Mercandelli, M.A. Ortenzi, G. Terraneo, C. Botta, R.T.K. Kwok, J.W.Y. Lam, B. Z. Tang, E. Cariati, Tunable linear and nonlinear optical properties from room temperature phosphorescent cyclic triimidazole-pyrene bio-probe, Chem. Eur. J. 27 (2021) 16690–16700, https://doi.org/10.1002/chem.202102839.
[20] D. Malpicci, S. Andolina, S. Di Ciolo, E. Lucenti, E. Cariati, S. Marzano, B. Pagano, J. Amato, A. Randazzo, C. Giannini, Cyclic triimidazoles as stabilizers for gene promoter and human telomeric DNA G-quadruplexes, Eur. J. Org. Chem. 2022 (2022), e202200718, https://doi.org/10.1002/ejoc.202200718.
[21] E. Lucenti, A. Forni, C. Botta, L. Carlucci, A. Colombo, C. Giannini, D. Marinotto, A. Previtali, S. Righetto, E. Cariati, The effect of bromo substituents on the multifaceted emissive and crystal-packing features of cyclic triimidazole derivatives, ChemPhotoChem 2 (2018) 801–805, https://doi.org/10.1002/cptc.201800151.
[22] K.L. Kirk, W. Nagai, L.A. Cohen, Photochemistry of diazonium salts. II. Synthesis of 2-fluoro-L-histidine and 2-fluorohistamine, and the halogen lability of 2-fluoroimidazoles, J. Am. Chem. Soc. 95 (1973) 8389–8392.
[23] D.M. Schubert, D.T. Natan, D.C. Wilson, K.I Hardcastle, Facile synthesis and structures of cyclic triiimidazole and its boric acid adduct, Cryst. Growth Des. 11 (2011) 843–850.
[24] E. Lucenti, A. Forni, C. Botta, C. Giannini, D. Malpicci, D. Marinotto, A. Previtali, S. Righetto, E. Cariati, Intrinsic and extrinsic heavy-atom effects on the multifaceted emissive behavior of cyclic triimidazole, Chem. Eur. J. 25 (2019) 2452–2456, https://doi.org/10.1002/chem.201804980.
[25] C. Giannini, A. Forni, D. Malpicci, E. Lucenti, D. Marinotto, A. Previtali, L. Carlucci, E. Cariati, room temperature phosphorescence from organic materials: unravelling the emissive behaviour of chloro-substituted derivatives of cyclic triimidazole, Eur. J. Org. Chem. 2021 (2021) 2041–2049, https://doi.org/10.1002/ejoc.202100131.
[26] E. Lucenti, A. Forni, A. Previtali, D. Marinotto, D. Malpicci, S. Righetto, C. Giannini, T. Virgili, P. Kabacinski, L. Ganzer, U. Giovanella, C. Botta, E. Cariati, Unravelling the intricate photophysical behavior of 3-(pyridin-2-yl) triimidazotriazine AIE and RTP polymorphs, Chem. Sci. 11 (2020) 7599–7608, https://doi.org/10.1039/d0sc02459g.
[27] A. Previtali, E. Lucenti, A. Forni, L. Mauri, C. Botta, C. Giannini, D. Malpicci, D. Marinotto, S. Righetto, E. Cariati, Solid State room temperature dual phosphorescence from 3-(2-Fluoropyridin-4-yl)triimidazo [1,2-a:1′,2′-c:1″,2″-e] [1,3,5]triazine, Molecules 24 (2019) 2552, https://doi.org/10.3390/molecules24142552.
[28] D. Malpicci, C. Giannini, E. Lucenti, A. Forni, D. Marinotto, E. Cariati, Mono-, Di., Tri-pyrene substituted cyclic triimidazole: a family of highly emissive and RTP chromophores, Photochem 1 (2021) 477–487, https://doi.org/10.3390/photochem1030031.
[29] D. Malpicci, A. Forni, E. Cariati, R. Inoguchi, D. Marinotto, D. Maver, F. Turco, E. Lucenti, Crystallization-enhanced emission and room-temperature phosphorescence of cyclic triimidazole-monohexyl thiophene derivatives, Molecules 28 (2023) 140.
[30] E. Melnic, V.C. Kravtsov, E. Lucenti, E. Cariati, A. Forni, N. Siminel, M.S. Fonari, Regulation of π···π stacking interactions between triimidazole luminophores and comprehensive emission quenching by coordination to Cu(II), New J. Chem. 45 (2021) 9040–9052, https://doi.org/10.1039/d1nj00909e.
[31] D. Malpicci, D. Blasi, D. Marinotto, A. Forni, E. Cariati, E. Lucenti, L. Carlucci, A rare structural motif for a luminescent Cu(I) coordination polymer with 3-(Pyridin-2- yl)triimidazotriazine, Crystals 13 (2023) 149.
[32] E. Cariati, A. Forni, E. Lucenti, D. Marinotto, A. Previtali, S. Righetto, C. Botta, V. Bold, V. Kravtsov, M.S. Fonari, Extrinsic heavy metal atom effect on the solid-state room temperature phosphorescence of cyclic triimidazole, Chem. Asian J. 14 (2019) 853–858, https://doi.org/10.1002/asia.201801604.
[33] M. Magni, E. Lucenti, A. Previtali, P.R. Mussini, E. Cariati, Electrochemistry of cyclic triimidazoles and their halo derivatives: a casebook for multiple equivalent centers and electrocatalysis, Electrochim. Acta 317 (2019) 272–280, https://doi.org/10.1016/j.electacta.2019.05.146.
[34] P.J. Elving, S.J. Pace, J.E. O'Reilly, Electrochemical reduction of purine, pyrimidine and imidazole in aqueous media. Kinetics and Mechanisms, J. Am. Chem. Soc. 95 (1973) 647–658.
[35] H.L. Wang, R.M. O'Malley, J.E. Fernandez, Electrochemical and chemical polymerization of imidazole and some of its derivatives, Macromolecules 27 (1994) 893–901.
[36] Y. Takeuchi, K.L. Kirk, L.A. Cohen, Imidazole Cyclotrimers (Trimidazoles), a Novel Heteroannular Series, J. Org. Chem. 44 (1979) 4234–4246.
[37] S. Arnaboldi, R. Cirilli, A. Forni, A. Gennaro, A.A. Isse, V. Mihali, P.R. Mussini, M. Pierini, S. Rizzo, F. Sannicolò, Electrochemistry and chirality in bibenzimidazole systems, Electrochim. Acta 179 (2015) 250–262.
[38] F.G. Guijarro, S.M. Rivero, S. Gunasekaran, I. Arretxea, R.P. Ortiz, R. Caballero, P. de la Cruz, F. Langa, L. Venkataraman, J. Casado, Synthesis and electronic properties of pyridine end-capped cyclopentadithiophene-vinylene oligomers, RSC Adv. 10 (2020) 41264–41271.
[39] J. Heinze, B.A. Frontana-Uribe, S. Ludwigs, Electrochemistry of conducting polymers-persistent models and new concepts, Chem. Rev. 110 (2010) 4724–4771.
[40] K. Meerholz, J. Heinze, Electrochemical solution and solid-state investigations on conjugated oligomers and polymers of the α-thiophene and the p-phenylene series, Electrochim. Acta 41 (1996) 1839–1854.
[41] M. Baghbanzadeh, C. Pilger, C. Oliver Kappe, Palladium-catalyzed direct arylation of heteroaromatic compounds: Improved conditions utilizing controlled microwave heating, J. Org. Chem. 76 (2011) 8138–8142, https://doi.org/10.1021/jo201516v.
[42] A.A. Isse, A. Gennaro, Absolute potential of the standard hydrogen electrode and the problem of interconversion of potentials in different solvents, J. Phys. Chem. B 114 (2010) 7894–7899.
[43] C. Hansch, A. Leo, R.W. Taft, A survey of Hammett substituent constants and resonance and field parameters, Chem. Rev. 91 (1991) 165–195.
[44] M. Charton, Electrical effects of ortho substituents in imidazoles and benzimidazoles, J. Org. Chem. 30 (1965) 3346–3350.
[45] P.R. Mussini, S. Arnaboldi, M. Magni, S. Grecchi, G. Longhi, T. Benincori, Enantiomer discrimination in absorption spectroscopy and in voltammetry: highlighting fascinating similarities and connections, Curr. Opin. Electrochem. 37 (2023), 101128.
[46] R.K. Konidena, K.R. Justin Thomas, S. Sahoo, D.K. Dubey, J..H. Jou, Multi-substituted deep-blue emitting carbazoles: a comparative study on photophysical and electroluminescence characteristics, J. Mater. Chem. C 5 (2017) 709–726, https://doi.org/10.1039/c6tc04870f.
[47] R.K. Konidena, K.R.J. Thomas, S. Kumar, Y.C. Wang, C.J. Li, J.H Jou, Phenothiazine decorated carbazoles: effect of substitution pattern on the optical and electroluminescent characteristics, J. Org. Chem. 80 (2015) 5812–5823.
[48] A. Lasia, Electrochemical Impedance Spectroscopy and its Applications, Springer, 2014.